A Printed-Circuit Hybrid-Ring Directional Coupler for Arbitrary Power Divisions

ASHOK K. AGRAWAL, SENIOR MEMBER, IEEE, AND GERALD F. MIKUCKI

Abstract—**A directional coupler in the form of a hybrid ring particularly suited for printed circuits is described. The maximum power-split ratio between the two output ports of a printed-circuit conventional hybrid-ring coupler is limited by the highest impedance line that can be realized [1]. The hybrid-ring directional coupler described in this paper allows a larger power-split ratio for the same impedance lines, and thereby increases the range of the power-split ratio that can be realized for printed circuits. A theoretical analysis was conducted using the scattering matrix, and experimental verification of the theoretical results was achieved in a stripline configuration at *Ku*-band.**

I. INTRODUCTION

THE HYBRID-RING directional coupler is an appealing choice for the basic power division element in beam-forming networks for printed-circuit array antennas for two primary reasons: 1) the output arms are isolated from each other, and 2) the input impedance is matched when the other arms are terminated by matched impedances. Since the conventional T (or Y) junction power dividers do not possess these properties, directional couplers are preferable for antenna array feed systems where the isolation between the output arms of the power divider is essential in order to minimize mutual coupling between radiating elements.

The two-dimensional structure of stripline facilitates construction of the feeding network and antenna elements, such as dipoles on a single printed circuit board. At high frequencies, limited real estate makes hybrid-ring couplers preferable to branch-line and parallel-line couplers; the former has an inherent 90° phase difference between the output ports. For an antenna array that is fed by an equiphase, symmetrical, corporate network, the hybrid-ring directional coupler has a definite advantage over the parallel-line and branch-line couplers because no phase-compensating element is necessary. The hybrid-ring coupler also has a broader bandwidth than the branch-line coupler [1].

The configuration of a conventional hybrid-ring directional coupler is shown in Fig. 1. The characteristic admittances of the four arms are normalized to unity. The variable parameters Y_1, and Y_2 represent the characteristic admittances of two lines of the ring. They determine the degree of coupling of the output arms and the matching condition for the input arm. When the signal is fed into sum port 3, the output voltages in arms 1 and 2 are in phase, and their relative amplitudes are related by

$$\frac{b_1}{b_2} = \frac{Y_2}{Y_1}. \tag{1}$$

When the signal is fed into difference port 1, the output voltages in arms 3 and 4 are 180° out of phase, and their relative amplitudes are related by

$$\frac{b_3}{b_4} = -\frac{Y_2}{Y_1}. \tag{2}$$

In both cases, the condition that the input arm be perfectly matched requires that Y_1 and Y_2 satisfy the condition

$$Y_1^2 + Y_2^2 = 1. \tag{3}$$

From (1) and (2), it is evident that the output voltage ratio is directly proportional to the ratio of the characteristic admittances (or impedances) of the transmission lines forming the ring. The impedance values required for various power-split ratios are presented in Table I. In microstrip and stripline circuits, the highest impedance line that can be realized limits the maximum power-split ratio between the two output arms. The highest attainable impedance value for striplines and microstrips is a function of the physical characteristics of the substrate (e.g., dielectric constant and thickness). The practical impedance limit for most substrates, using conventional etching techniques, is around 150 Ω. Referring to Table I, this limits the maximum power-split ratio for a conventional hybrid-ring coupler to approximately 9 dB.

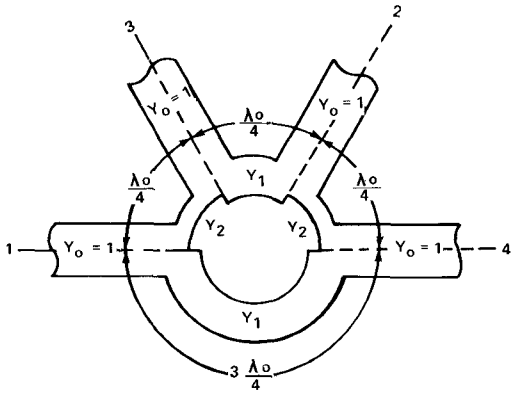

Fig. 1. Conventional hybrid-ring directional coupler.

Manuscript received April 3, 1986; revised July 1, 1986.

The authors are with the RCA Missile and Surface Radar Division, Moorestown, NJ 08057.

IEEE Log Number 8610548.

TABLE I
CHARACTERISTIC IMPEDANCES OF THE LINES FOR TWO HYBRID-RING DIRECTIONAL COUPLERS

	CONVENTIONAL HYBRID RING		MODIFIED HYBRID RING	
POWER-SPLIT RATIO (dB)	Z_1	Z_2	Z_1	Z_2
0 0	70 7	70 7	70 7	70 7
1 0	75 1	67 0	72 3	66 9
2 0	80 4	63 9	74 5	63 8
3.0	86 5	61 3	77 3	61 1
4 0	93 7	59 1	80 8	59 0
5 0	102 0	57 4	84 9	57.1
6 0	111 6	55.9	89.8	55.6
7 0	122 6	54 8	95 6	54.4
8 0	135 2	53 8	102 3	53 5
9 0	149 5	53.1	109.9	52 7
10 0	165 8	52 4	118 6	52.1
11.0	184 3	51 9	128 4	51 6
12 0	205 2	51 6	139 4	51 2
13 0	228 9	51 2	151 9	50 9
14 0	255 5	51.0	165 9	50.7
15 0	285 6	50.8	181 6	50 5

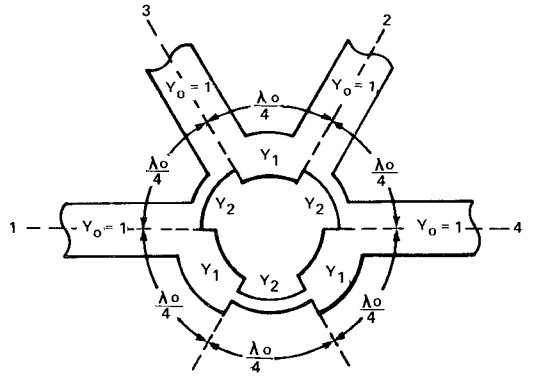

Fig. 2. Modified hybrid-ring directional coupler.

To obtain a higher power-split ratio between the output ports, the three-quarter-wavelength line in the ring is split into three one-quarter-wavelength lines of characteristic admittances Y_1 and Y_2, as illustrated in Fig. 2. This modified hybrid-ring directional coupler was analyzed using the scattering matrix for the four-port devices. Experimental results for two stripline couplers with power-split ratios of 6.4 and 11.3 dB are presented in this paper. The modified hybrid ring is similar to the conventional hybrid ring in that (a) its input impedance is matched when the two adjacent arms are terminated by matched loads and (b) the voltages in the two output arms are either in phase or 180° out of phase, depending on the input arm chosen. The power-split ratio is adjusted by varying the impedances of the lines in the ring between the arms.

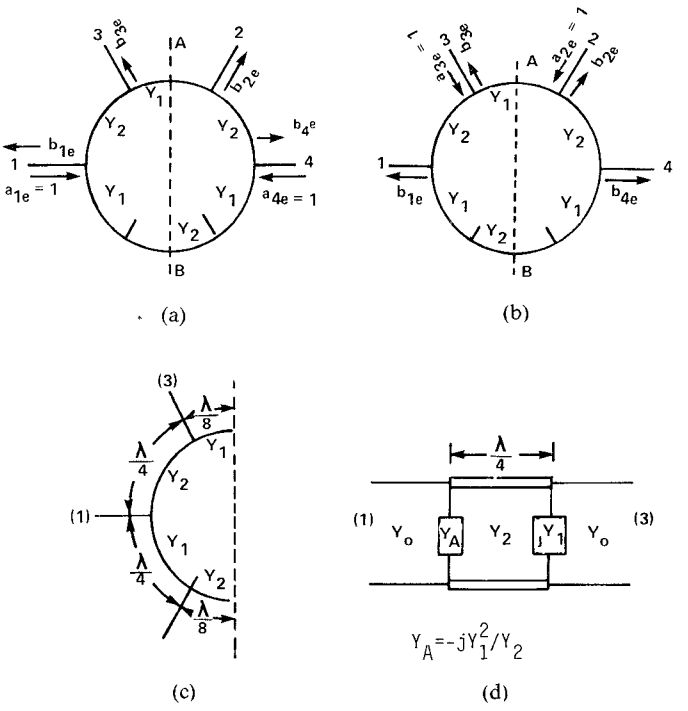

Fig. 3. Even mode. (a) Incident waves at arms 1 and 4. (b) Incident waves at arms 2 and 3. (c) Open circuit at $A-B$. (d) Equivalent circuit.

The modified hybrid-ring coupler differs from the conventional ring coupler in that the two output arms are not perfectly isolated at the center frequency, but it provides sufficient isolation over a frequency band to satisfy requirements for most applications.

II. Analysis of the Hybrid-Ring Directional Coupler

The configuration of the modified hybrid-ring directional coupler is illustrated in Fig. 2. The characteristic admittances of the four arms are equal and normalized to unity. The variable parameters are the two characteristic admittances Y_1 and Y_2 of the quarter-wave lines of the ring; these two admittances determine the power-split ratio between the two output arms and the impedance-matching condition for the input arm.

The modified hybrid-ring coupler was analyzed by using the procedure for the analysis of symmetrical four-port networks [1], [2] and by reducing the four-port network to a two-port network by taking advantage of the symmetry about the plane $A-B$. When two in-phase waves of unit amplitude are applied to terminals 1 and 4 or to terminals 2 and 3, the current is zero at the plane $A-B$. As a result, the ring can be open-circuited at this plane, and only one-half of the circuit needs to be analyzed. This condition is referred to as the even mode, and all parameters associated with this mode are denoted by subscript e (see Fig. 3). Similarly, when two opposite-phase waves of unit amplitude are applied to terminals 1 and 4 or to terminals 2 and 3, the voltage is zero at the plane $A-B$. As a result, the ring can be short-circuited at this plane, and only one-half of the circuit needs to be analyzed. This condition is referred to as the odd mode, and all parameters associated

with this mode are identified by the subscript o (Fig. 4). The equivalent circuits for these two modes are shown in Figs. 3(d) and 4(d), respectively.

In Fig. 3(d), the shunt admittance Y_A is the admittance at the input of a $\lambda/4$ line of characteristic admittance Y_1, which is connected to an open-circuited $\lambda/8$ line of characteristic admittance Y_2. Similarly, in Fig. 4(d), the shunt admittance Y_B is the admittance at the input of a $\lambda/4$ line of characteristic admittance Y_1, which is connected to a short-circuited $\lambda/8$ line of characteristic admittance Y_2. Y_A and Y_B are given by

$$Y_A = -\frac{jY_1^2}{Y_2} \tag{4}$$

$$Y_B = \frac{jY_1^2}{Y_2}. \tag{5}$$

The reflected waves in each arm are calculated from the scattering matrices for the even and odd modes. The superposition of the two waves of the two modes results in a single incident wave in one arm.

III. Scattering Matrices for the Even and Odd Modes

The scattering matrix for each mode can be determined from the admittance matrix for each mode [3]. The scattering matrix is related to the admittance matrix by

$$[S] = [I - Y][I + Y]^{-1} \tag{6}$$

where $[I]$ is an identity matrix.

The admittance matrices for even and odd modes are the admittance matrices of the two-port networks in Figs. 3(d) and 4(d). The admittance matrices for even and odd modes are given by

$$[Y]_e = j\begin{bmatrix} -Y_1^2/Y_2 & Y_2 \\ Y_2 & Y_1 \end{bmatrix} \tag{7}$$

$$[Y]_o = j\begin{bmatrix} Y_1^2/Y_2 & Y_2 \\ Y_2 & -Y_1 \end{bmatrix}. \tag{8}$$

Substitution of (7) and (8) into (6) yields the scattering matrices for even and odd modes, which are given by

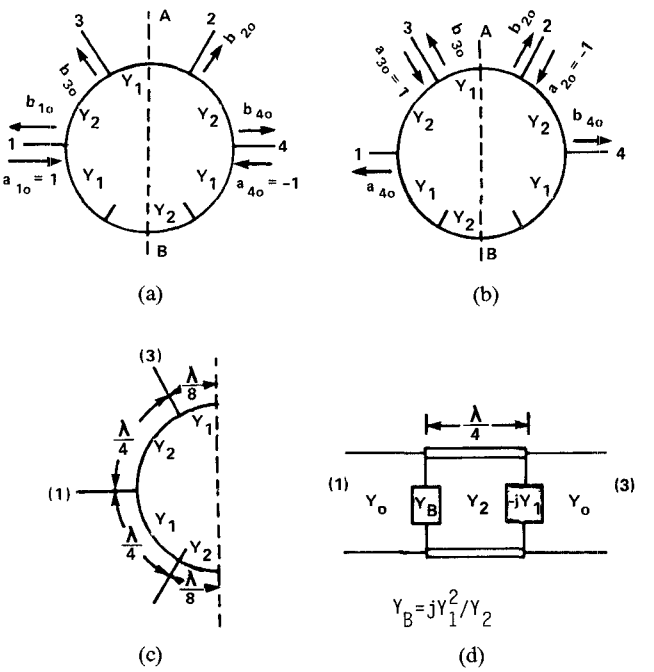

Fig. 4. Odd mode. (a) Incident waves at arms 1 and 4. (b) Incident waves at arms 2 and 3. (c) Short circuit at $A-B$. (d) Equivalent circuit.

Recalling that the reflected waves are related to the incident waves by

$$[b] = [S][a] \tag{11}$$

we can now determine the reflected wave in each arm for each mode. For the first case, in which the incident waves are at arms 1 and 4, the reflected waves for the even mode are

$$b_{1e} = b_{4e} = \frac{1 - Y_2^2 - Y_1^3/Y_2 + j\left(Y_1 + Y_1^2/Y_2\right)}{1 + Y_2^2 + Y_1^3/Y_2 + j\left(Y_1 - Y_1^2/Y_2\right)} \tag{12}$$

$$b_{2e} = b_{3e} = \frac{-2jY_2}{1 + Y_2^2 + Y_1^3/Y_2 + j\left(Y_1 - Y_1^2/Y_2\right)}. \tag{13}$$

For the odd mode, the reflected waves are

$$b_{1o} = -b_{4o} = \frac{1 - Y_2^2 - Y_1^3/Y_2 - j\left(Y_1 + Y_1^2/Y_2\right)}{1 + Y_2^2 + Y_1^3/Y_2 - j\left(Y_1 - Y_1^2/Y_2\right)} \tag{14}$$

$$b_{2o} = -b_{3o} = \frac{2jY_2}{1 + Y_2^2 + Y_1^3/Y_2 - j\left(Y_1 - Y_1^2/Y_2\right)}. \tag{15}$$

$$[S]_e = \begin{bmatrix} \dfrac{1 - Y_2^2 - Y_1^3/Y_2 + j\left(Y_1 + Y_1^2/Y_2\right)}{1 + Y_2^2 + Y_1^3/Y_2 + j\left(Y_1 - Y_1^2/Y_2\right)} & \dfrac{-2jY_2}{1 + Y_2^2 + Y_1^3/Y_2 + j\left(Y_1 - Y_1^2/Y_2\right)} \\ \dfrac{-2jY_2}{1 + Y_2^2 + Y_1^3/Y_2 + j\left(Y_1 - Y_1^2/Y_2\right)} & \dfrac{1 - Y_2^2 - Y_1^3/Y_2 - j\left(Y_1 + Y_1^2/Y_2\right)}{1 + Y_2^2 + Y_1^3/Y_2 + j\left(Y_1 - Y_1^2/Y_2\right)} \end{bmatrix} \tag{9}$$

$$[S]_o = \begin{bmatrix} \dfrac{1 - Y_2^2 - Y_1^3/Y_2 - j\left(Y_1 + Y_1^2/Y_2\right)}{1 + Y_2^2 + Y_1^3/Y_2 - j\left(Y_1 - Y_1^2/Y_2\right)} & \dfrac{-2jY_2}{1 + Y_2^2 + Y_1^3/Y_2 - j\left(Y_1 - Y_1^2/Y_2\right)} \\ \dfrac{-2jY_2}{1 + Y_2^2 + Y_1^3/Y_2 - j\left(Y_1 - Y_1^2/Y_2\right)} & \dfrac{1 - Y_2^2 - Y_1^3/Y_2 + j\left(Y_1 + Y_1^2/Y_2\right)}{1 + Y_2^2 + Y_1^3/Y_2 - j\left(Y_1 - Y_1^2/Y_2\right)} \end{bmatrix} \tag{10}$$

When the even and odd modes are superimposed, the resultant waves are given by

$(a_1 = 2,\ a_4 = 0)$

$$b_1 = \frac{2\left[1-\left(Y_2^2+Y_1^3/Y_2\right)^2+\left(Y_1^2-Y_1^4/Y_2^2\right)\right]}{\left(1+Y_2^2+Y_1^3/Y_2\right)^2+\left(Y_1-Y_1^2/Y_2\right)^2} \quad (16)$$

$$b_2 = \frac{-4Y_2\left(Y_1-Y_1^2/Y_2\right)}{\left(1+Y_2^2+Y_1^3/Y_2\right)^2+\left(Y_1-Y_1^2/Y_2\right)^2} \quad (17)$$

$$b_3 = \frac{-4jY_2\left(1+Y_2^2+Y_1^3/Y_2\right)}{\left(1+Y_2^2+Y_1^3/Y_2\right)^2+\left(Y_1-Y_1^2/Y_2\right)^2} \quad (18)$$

$$b_4 = \frac{4jY_1\left(Y_1/Y_2+Y_2^2+Y_1^3/Y_2\right)}{\left(1+Y_2^2+Y_1^3/Y_2\right)^2+\left(Y_1-Y_1^2/Y_2\right)^2}. \quad (19)$$

Similarly, for the second case, in which the incident waves are at arms 3 and 2, the reflected waves for the even mode are

$$b_{1e} = b_{4e} = \frac{-2jY_2}{1+Y_2^2+Y_1^3/Y_2+j\left(Y_1-Y_1^2/Y_2\right)} \quad (20)$$

$$b_{3e} = b_{2e} = \frac{1-Y_2^2-Y_1^3/Y_2-j\left(Y_1+Y_1^2/Y_2\right)}{1+Y_2^2+Y_1^3/Y_2+j\left(Y_1-Y_1^2/Y_2\right)}. \quad (21)$$

The reflected waves for the odd mode are

$$b_{1o} = -b_{4o} = \frac{-2jY_2}{1+Y_2^2+Y_1^3/Y_2-j\left(Y_1-Y_1^2/Y_2\right)} \quad (22)$$

$$b_{3o} = -b_{2o} = \frac{1-Y_2^2-Y_1^3/Y_2+j\left(Y_1+Y_1^2/Y_2\right)}{1+Y_2^2+Y_1^3/Y_2-j\left(Y_1-Y_1^2/Y_2\right)}. \quad (23)$$

The resultant waves when the even and odd modes are superimposed are given by

$$a_3 = 2,\ a_2 = 0 \quad (24)$$

$$b_1 = \frac{-4jY_2\left(1+Y_2^2+Y_1^3/Y_2\right)}{\left(1+Y_2^2+Y_1^3/Y_2\right)^2+\left(Y_1-Y_1^2/Y_2\right)^2} \quad (25)$$

$$b_2 = \frac{-4jY_1\left[1+\left(Y_1/Y_2\right)\left(Y_2^2+Y_1^3/Y_2\right)\right]}{\left(1+Y_2^2+Y_1^3/Y_2\right)^2+\left(Y_1-Y_1^2/Y_2\right)^2} \quad (26)$$

$$b_3 = \frac{2\left[1-\left(Y_2^2+Y_1^3/Y_2\right)^2-\left(Y_1^2-Y_1^4/Y_2^2\right)\right]}{\left(1+Y_2^2+Y_1^3/Y_2\right)^2+\left(Y_1-Y_1^2/Y_2\right)^2} \quad (27)$$

$$b_4 = \frac{-4Y_2\left(Y_1-Y_1^2/Y_2\right)}{\left(1+Y_2^2+Y_1^3/Y_2\right)^2+\left(Y_1-Y_1^2/Y_2\right)^2}. \quad (28)$$

The resultant waves for the two cases referred to as difference and sum modes are summarized in Fig. 5(a) and (b). The output voltage ratio between arms 3 and 4 for the difference mode in Fig. 5(a) is given by

$$\frac{b_3}{b_4} = -\frac{Y_2\left(1+Y_2^2+Y_1^3/Y_2\right)}{Y_1\left(Y_1/Y_2+Y_2^2+Y_1^3/Y_2\right)} \quad (29)$$

and the output voltage ratio between arms 1 and 2 for this

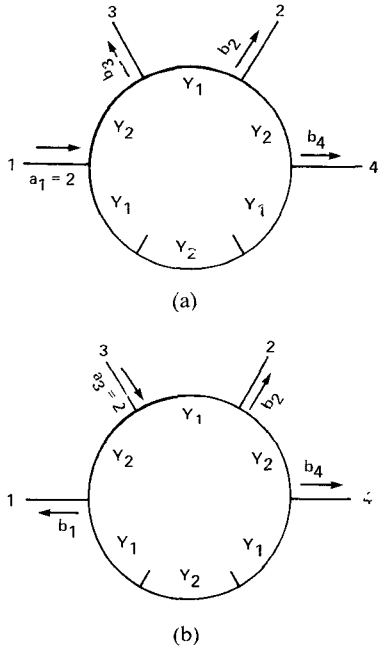

Fig. 5. Incident and reflected waves for the (a) difference and (b) sum modes.

sum mode in Fig. 5(b) is given by

$$\frac{b_1}{b_2} = \frac{Y_2\left(1+Y_2^2+Y_1^3/Y_2\right)}{Y_1\left[1+Y_1/Y_2\left(Y_2^2+Y_1^3/Y_2\right)\right]}. \quad (30)$$

The condition that the input arm in both cases be matched requires that b_1 in (16) and b_3 in (27) be zero. A close look at (16) and (27) indicates that a perfect match condition cannot be obtained simultaneously at both ports 1 and 3. A near perfect match is achieved at ports 1 and 3 for the following condition:

$$Y_2^2 + \frac{Y_1^3}{Y_2} = 1. \quad (31)$$

When Y_1 and Y_2 satisfy this condition, the resultant reflected waves in (16) and (27) are given by

$$b_1 = \frac{2\left(Y_1^2-Y_1^4/Y_2^2\right)}{\left(1+Y_2^2+Y_1^3/Y_2\right)^2+\left(Y_1-Y_1^2/Y_2\right)^2}$$

(difference mode) (32)

$$b_3 = -\frac{2\left(Y_1^2-Y_1^4/Y_2^2\right)}{\left(1+Y_2^2+Y_1^3/Y_2\right)^2+\left(Y_1-Y_1^2/Y_2\right)^2}$$

(sum mode) (33)

and the output voltage ratio between arms 3 and 4 for the difference mode and arms 1 and 2 for the sum mode are given by

$$\frac{b_3}{b_4} = -\frac{2Y_2}{Y_1\left(1+Y_1/Y_2\right)} \quad (34)$$

$$\frac{b_1}{b_2} = \frac{2Y_2}{Y_1\left(1+Y_1/Y_2\right)}. \quad (35)$$

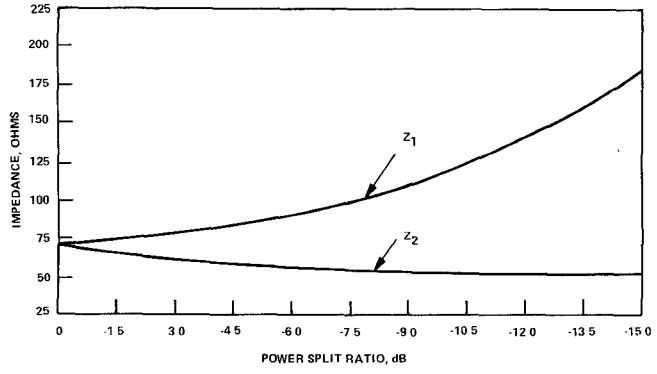

Fig. 6. Characteristic impedances of the transmission lines versus power-split ratios.

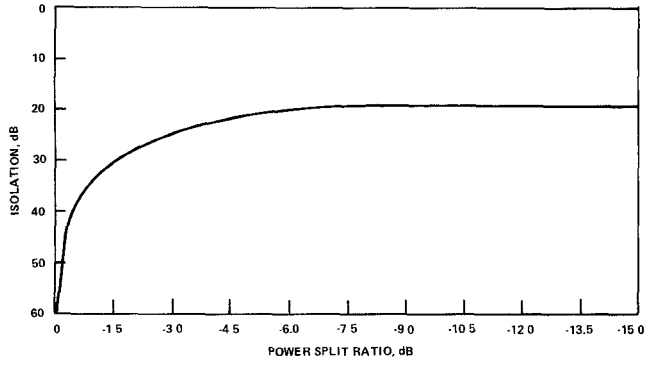

Fig. 7. Isolation between the output ports versus power-split ratios.

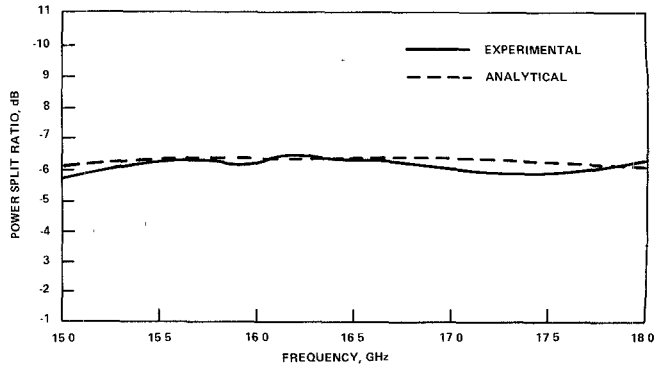

(a)

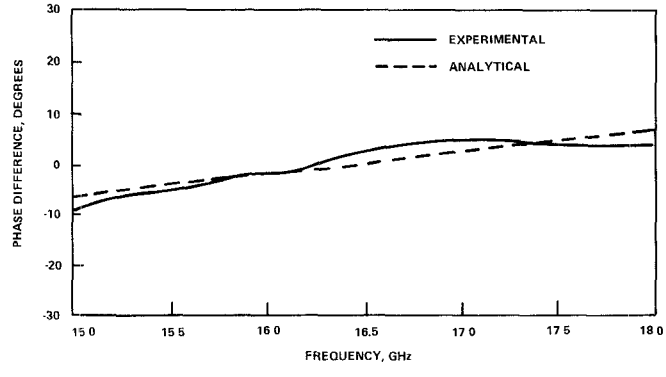

(b)

Fig. 8. (a) Power-split ratio between ports 1 and 2 of the 6.4-dB hybrid-ring coupler. (b) Phase difference between ports 1 and 2 of the 6.4-dB hybrid-ring coupler.

Equation (34) states that for an input voltage at arm 1, the output voltages at arms 3 and 4 are 180° out of phase. Equation (35) states that for an input voltage at arm 3, the output voltages at arms 1 and 2 are in phase. The characteristic impedance values Z_1 and Z_2 for various power-split ratios between the output ports are tabulated in Table I for comparison with the conventional hybrid-ring coupler.

The magnitude of the reflected waves in (32) and (33) for values of Y_1 and Y_2 corresponding to the characteristic impedances in Table I for various power-split ratios is very small; it results in a voltage standing wave ratio (VSWR) of less than 1.1 for smaller power-split ratios and decreases to 1.05 for higher power-split ratios, establishing the useful range for this directional coupler. By symmetry, if the input waves are incident at ports 4 and 2, the reflected wave amplitudes will be the same as in (32) and (33), respectively. Thus, the input impedance at any port is matched (VSWR <1.1) when the other arms are terminated by matched impedances.

The characteristic impedance values Z_1 and Z_2 for various power-split ratios and the isolation values between output ports for the sum mode are plotted in Figs. 6 and 7, respectively. The isolation between the output ports is about 20 dB for power-split ratios of less than -6 dB. As the power-split ratio approaches zero dB (equal split, "rat-race" ring), the isolation approaches infinity.

Although the theoretical isolation between the output ports for the modified hybrid ring is of the order of 20 dB, as compared to the infinite isolation for the conventional hybrid ring, the average difference between the measured results over a frequency band for the two cases is approximately 5 dB. A 20-dB isolation is adequate for most applications.

Comparing the impedance for the modified hybrid ring and for the conventional ring (Table I), the range of the realizable power-split ratios is significantly increased for the same realizable impedance values. For example, for a power-split ratio of 8 dB, the conventional ring requires a line of impedance 135.2 Ω, while for a 12-dB power-split ratio, the modified ring requires a line of impedance 139.4 Ω. Thus, the realizable range of power-split ratios for the modified hybrid-ring directional coupler is increased by approximately 4 dB.

The results obtained above are for a single frequency. To find the frequency dependence of this hybrid coupler, it is necessary to consider the variations in the lengths of the quarter-wave lines with the frequency in the equivalent circuits. The frequency characteristics of this hybrid-ring coupler were obtained by analyzing the circuit on MIDAS (a computer program for analyzing microwave circuits) [4]. The power-split ratios, isolation between ports, phase difference between output ports, and input VSWR for two rings with power-split ratios of 6.4 dB and 11.3 dB are plotted in Figs. 8 through 11 as a function of frequency (15–18 GHz), along with the experimental results discussed in the next section. From these figures, we note that

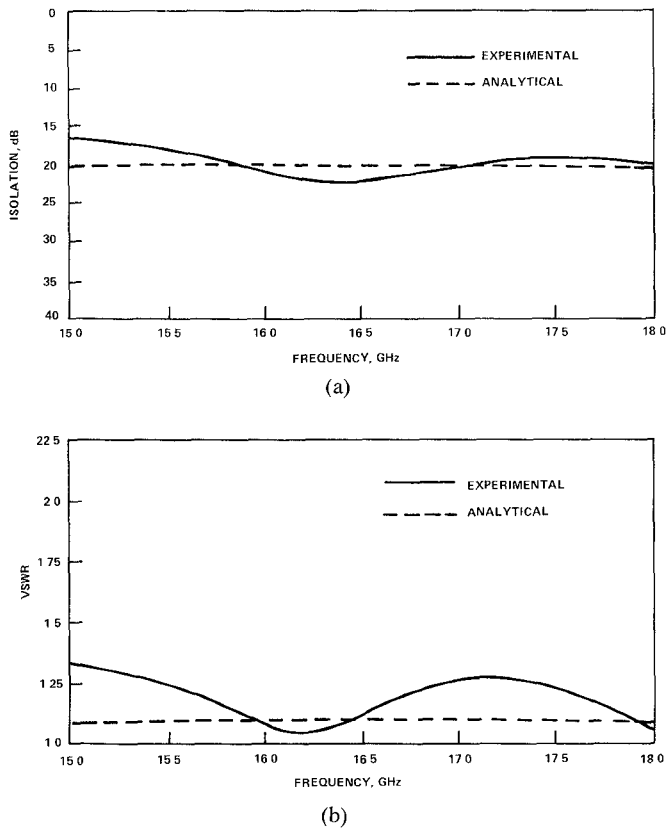

Fig. 9. (a) Isolation between ports 1 and 2 of the 6.4-dB hybrid-ring coupler. (b) Input VSWR at port 3 of the 6.4-dB hybrid-ring coupler.

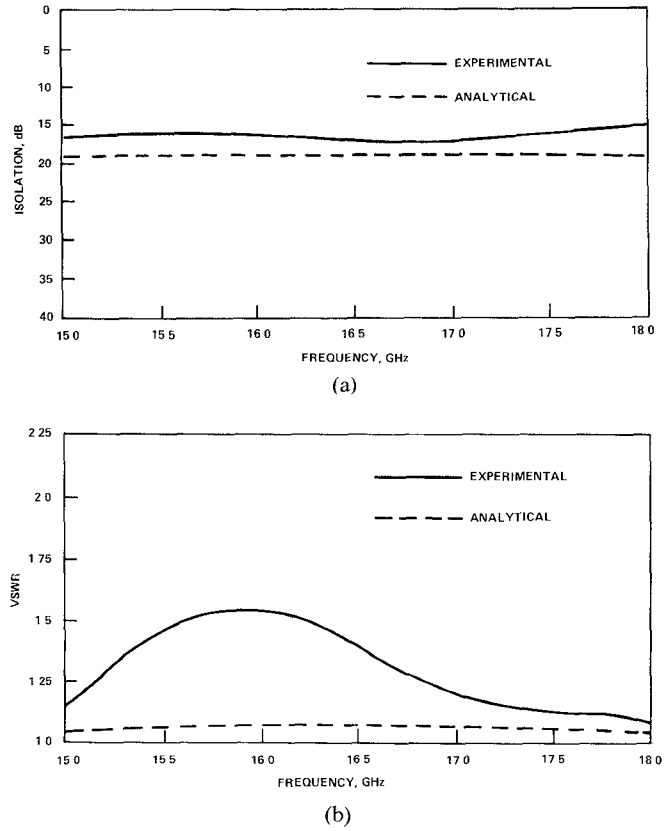

Fig. 11. (a) Isolation between ports 1 and 2 of the 11.3-dB hybrid-ring coupler. (b) Input VSWR at port 3 of the 11.3-dB hybrid-coupler.

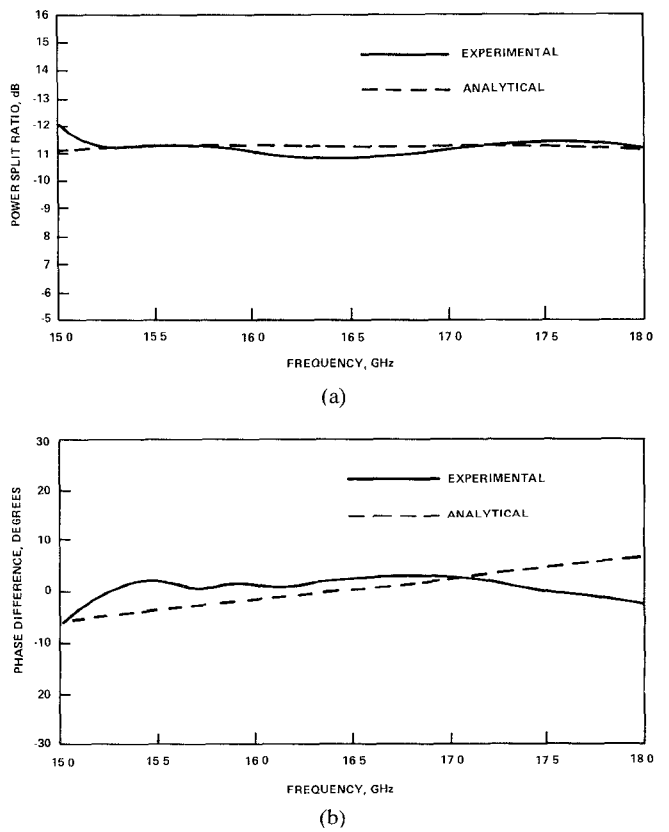

Fig 10. (a) Power-split ratio between ports 1 and 2 of the 11.3-dB hybrid-ring coupler. (b) Phase difference between ports 1 and 2 of the 11.3-dB hybrid-ring coupler.

the hybrid-ring coupler has a bandwidth of approximately 20 percent at *Ku*-band.

IV. Experimental Results

Two stripline hybrid-ring directional couplers with power-split ratios of 6.4 dB and 11.3 dB between the two output arms 1 and 2 (sum mode) at the center frequency of 16.5 GHz were designed and tested. The impedance values used for these two rings are (a) 6.4 dB coupler, $Z_1 = 92.0\ \Omega$ and $Z_2 = 55.1\ \Omega$, and (b) 11.3 dB coupler, $Z_1 = 131.6\ \Omega$ and $Z_2 = 51.5\ \Omega$. The measured power-split ratios, isolation, and phase difference between the output ports and input VSWR, along with the analytical results, are shown in Figs. 8 through 11. A close agreement between the analytical and experimental results is observed over the frequency range of 15 to 18 GHz. The input port is fairly well matched, with a VSWR of less than 1.5:1 over the frequency band.

The stripline hybrid rings were fabricated on a 50-mil Duroid 5880 substrate. Duroid 5880 substrate has a dielectric constant of 2.2 and provides low circuit loss.

V. Conclusions

The analysis and design of a hybrid-ring directional coupler that provides a higher power-split ratio than the conventional hybrid-ring coupler are presented. The measured results for two couplers developed in stripline configuration at *Ku*-band agree well with the analytical re-

sults. The hybrid-ring directional coupler has a bandwidth of approximately 20 percent. The input arm of the coupler is matched (VSWR $<1.5:1$) over the frequency band. The power-split ratio can be adjusted by varying the characteristic impedances (Z_1 and Z_2) of the two lines forming the ring. Similar hybrid-ring directional couplers can also be realized in microstrip configuration.

Acknowledgment

The authors would like to acknowledge several helpful discussions with F. Lalezari of Ball Aerospace Corporation, and thank V. Zvanya for his contributions in the fabrication of the hybrid rings.

References

[1] C. Y. Pon, "Hybrid-ring directional coupler for arbitrary power division," *IEEE Trans. Microwave Theory Tech.*, vol. MTT-9, pp. 529–535, Nov. 1961.

[2] J. Reed and G. J. Wheeler, "A method of analysis of symmetrical four-port networks," *IEEE Trans. Microwave Theory Tech.*, vol. MTT-4, pp. 246–252, Oct. 1956.

[3] R. E. Collin, *Foundations for Microwave Engineering*. New York. McGraw-Hill, 1966.

[4] D. Rhodes and S. Perlow, "'MIDAS,' A new microwave RF CAD program," in *1985 Int. Symp. Microwave Theory Tech. Dig.*, pp. 707–710.

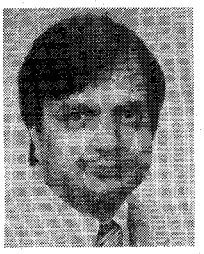

Ashok K. Agrawal (S'76–M'80–SM'82) received the M.S. and Ph.D. degrees in electrical engineering from the University of New Mexico, Albuquerque, in 1976 and 1979, respectively.

From 1973 to 1974, he was a Research Fellow at the Indian Institute of Technology, Kharagpur, India. From 1976 to 1982, he worked as a research scientist at Mission Research Corporation in Albuquerque and from 1982 to 1983 as a senior research engineer at Dikewood Corporation in Albuquerque. During 1982–1983, he also was an adjunct faculty member at the University of New Mexico, where he taught graduate courses on antennas. In 1983, he joined the Missile and Surface Radar Division of RCA Corporation in Moorestown, NJ, as a principal member of the engineering staff. Since then, he has been involved in research and development work on phased-array and microwave antennas.

Dr. Agrawal has published and presented over 25 papers on printed-circuit antennas, microwave circuits, multiconductor transmission lines, electromagnetic coupling, lightning, and emp. He was vice chairman of the APS/MTTS/EMC Albuquerque chapter during 1982–1983, and is currently chairman of the APS/MTTS Philadelphia chapter. Dr. Agrawal is a member of Tau Beta Pi.

Gerald F. Mikucki was born in Point Pleasant, NJ, in February 1961. In 1983, he received the B.S.E.E. degree from Pennsylvania State University.

From 1983 to 1985, he was with the Combat Surveillance and Target Acquisition Laboratory, Fort Monmouth, NJ, where he was involved in the development of electronic scan techniques for millimeter-wave antennas. Since 1985, he has been with the Missile and Surface Radar Division of RCA Corporation in Moorestown, NJ, where he is actively involved in the design and development of microwave circuits and antennas.